THEORETICAL H-BETA LINE PROFILES AND RELATED PARAMETERS FOR ROTATING B STARS

GEORGE W. COLLINS II AND J. PATRICK HARRINGTON
Perkins Observatory, The Ohio State and Ohio Wesleyan Universities
Received March 10, 1966

ABSTRACT

This paper presents a method for the calculation of Hβ line profiles for rotating stars. Results are presented for a series of models spanning the B spectral class. In addition to the profiles, equivalent widths, photometric β-indices, and UBV colors are presented. Families of models are formed by using the results of recent studies of rotating stellar interiors, and variation of the line parameters due to effects of rotation are quantitatively calculated.

Macroscopic effects on the star, such as shape distortion, aspect effects, gravity darkening, limb darkening, and latitude variation of atmospheric parameters, are included. Microscopic effects dealing with the line formation, such as pure absorption, non-coherent resonance scattering, and coherent electron scattering, are also included. It was found that the inclusion of resonance scattering as a source of opacity is important if accurate rotational profiles are to be obtained.

Results are presented that demonstrate 50 per cent variation in Hβ equivalent widths resulting from rotation for stars of the same $(U - B)_0$. However, the effects of rotation on a color-color diagram are such as to move the model down the main sequence rather than away from it. An attempt is made to explain the observed correlation between variations in the photometric β-indices and $v_e \sin i$. It is suggested that an increased number of observations of rotating B stars may enable one to determine the extent to which differential rotation is present in these stars.

I. INTRODUCTION

Since the discovery that the phenomenon of axial rotation was actually present in a large number of stars, a great amount of effort has been spent in determining the effects of such rotation upon spectral lines. The early work of Carrol (1928, 1933) described an elegant mathematical formulation of a geometrical interpretation of the problem. Later Shajn and Struve (1929) developed a simple geometrical approach that enabled them to integrate a line profile over the surface of a rapidly rotating star. This method has been used extensively by Slettebak (1949, 1956) and others to determine $v_e \sin i$ from observationally obtained line profiles. Unfortunately, the method of Shajn and Struve only enables one to include the variation of physical parameters over the surface of a rapidly rotating star through use of a limb-darkening coefficient. The limb-darkening coefficient merely plays the role of a weighting factor to the intensity and is not usually taken to be a function of wavelength. Thus, no changes in the shape of the line profile, due to variation of the physical parameters on the stellar surface, can be included.

It has been demonstrated by several authors (e.g., Eddington 1926; Slettebak 1949) that physical parameters defining a stellar atmosphere may be expected to vary extensively over the surface of a rapidly rotating star. Recently, Abt and Osmer (1965) attempted to estimate the effects of a few of these parameters on the lines of hydrogen. However, they were not able to include even a majority of such physical variations, as this would require complete knowledge of the physical structure of a rotating stellar atmosphere.

Using the work of Von Zeipel (1924) and following some of the ideas of Slettebak (1949), one of the present authors (Collins 1963, 1965; henceforth referred to as "Papers I and II," respectively) estimated the variation of the physical parameters defining a model stellar atmosphere over the surface of a rapidly rotating star. The advent of large digital computers has enabled the accurate numerical integration, required to find the specific intensity and observed flux from a model rotating stellar atmosphere, to be carried out.

Recent advances in the theory of rotating stellar interiors have enabled the authors to eliminate some objectionable assumptions present in Papers I and II. Thus, it has finally become feasible to investigate the effects of stellar axial rotation on spectral lines whose profiles are quite sensitive to the physical structure of the stellar atmosphere.

This study is divided into three main sections. Section II will deal with the construction of the models used and the formation of the integrated specific intensity in the line and the relevant line profiles. Section III will be concerned with the intercomparison of various models by means of the rotating interior studies of Roxburgh, Griffith, and Sweet (1965). Since the comparison has been put on a more physical basis than that used in Papers I and II, some detailed comparison to observation can be made and this is the subject of the last two sections.

II. CONSTRUCTION OF THE MODEL AND CALCULATION OF THE LINE PROFILES AND RELATED PARAMETERS

In this section we shall consider the problem of the calculation of the line profile and associated quantities for a hydrogen line arising in the atmosphere of a rapidly rotating star. Such a calculation requires that we determine the atmospheric parameters determining the structure of a rapidly rotating stellar atmosphere. In order to do this we shall make the same assumptions as those made in Paper II. That is, (1) the potential field is that of a rapidly rotating Roche model; (2) the flux at any point on the surface of the rotating star will be proportional to the local gravity.

The validity of these assumptions are discussed at some length in Paper II. Following the development in Paper II, we arrive at the following equation for the effective temperature and surface gravity on the surface of the star having an angular velocity ω:

$$T_e^4(\omega,\theta) = \frac{L(\omega)}{4\pi\sigma R_p^2(\omega)}\, g_n(\mathfrak{w},\theta) C_n(\mathfrak{w}), \tag{1}$$

$$g(\omega,\theta) = \frac{GM}{R_p^2(\omega)}\, g_n(\mathfrak{w},\theta), \tag{2}$$

where

$$g_n(\mathfrak{w},\theta) = \left\{\left[\frac{1}{x^2(\theta)} - \tfrac{8}{27}\mathfrak{w}^2 x^2(\theta)\sin^2(\theta)\right]^2 + \left[\tfrac{8}{27}\mathfrak{w}^2 x(\theta)\sin\theta\cos\theta\right]^2\right\}^{1/2} \tag{3}$$

and

$$C_n(\mathfrak{w}) = \left[\int_0^1 \frac{g_n(\mathfrak{w},\theta)\, x^2(\theta)\, d(\cos\theta)}{|\boldsymbol{g}_n \cdot \boldsymbol{r}|}\right]^{-1}. \tag{4}$$

The definitions of $x(\theta)$ and $\mathfrak{w}$ are those used in both Papers I and II, namely,

$$\mathfrak{w}^2 = 27R_p^3(0)\omega^2/8\,GM \tag{5}$$

and

$$1 = \frac{1}{x(\theta)} + \tfrac{4}{27}\mathfrak{w}^2 x^2(\theta)\sin^2\theta\,. \tag{6}$$

We shall call equations (3), (4), and (6) the shape equations, as they essentially depend only on the geometry of the problem and not on any physical parameter. Under the assumption of constant polar radius (i.e., $R_p = R_p(0)$), $\mathfrak{w}$ may be interpreted as the fraction of angular velocity of breakup at which the model is rotating. However, as we shall see in § III, if the polar radius of the models of given mass depends on angular velocity, then this interpretation is no longer valid.

Using equations (1) and (2) and a predetermined chemical composition we may now turn to the determination of the atmosphere of the rotating star. In order to do this, we make the further assumption that the atmosphere appropriate for a rapidly rotating

star is a plane-parallel atmosphere given by the local physical conditions. In this work the same atmospheres were used as those in Paper II, and the method of obtaining the appropriate atmosphere is identical. Thus, having obtained a description of the physical parameters governing the flow of radiation through the outer layers of such a model, we may turn to the calculation of the line-absorption coefficient and the formation of the line profiles.

III. CONSTRUCTION OF MODELS AND FORMATION OF LINE STRENGTHS AND LINE PROFILES

a) The Line Absorption Coefficient

The first step in the calculation of a line profile is the formulation of the line absorption coefficient appropriate for the line in question. The line absorption coefficient for Hβ is given by Underhill (1951) as

$$(l_\nu + \iota_\nu) = \frac{\pi e^2 \lambda^2}{m c^2 F_0} f_\pm N_2 S(\alpha)(1 - e^{-h\nu/kT}), \tag{7}$$

where $f_\pm$ is the f-value of the Stark-shifted components of the line, $S(\alpha)$ is the shape function for the Stark-broadening mechanism, F_0 is the normal field strength, and N_2 is the number of hydrogen atoms in the second level of excitation per gram of stellar material. The absorption coefficient has been written as the sum of the pure absorption coefficient (l_ν) and the coefficient of non-coherent resonant scattering (ι_ν) in anticipation of our discussion of the line source function. F_0 is given by

$$F_0 = 2.61\, e(N^*)^{2/3}. \tag{8}$$

The number of ions per cubic centimeter (N^*) may be found directly from the electron pressure and temperature distributions of the model atmospheres through the use of the ideal-gas law:

$$N^* = N_e = P_e/kT. \tag{9}$$

A complete discussion of the recent work on the Stark-broadening function [$S(\alpha)$] can be found in the book by Griem (1964). This function is given in terms of the parameter $\alpha = \Delta\lambda/F_0$, where $\Delta\lambda$ is the distance from the central frequency in angstroms. Near the line center ($\alpha < 0.35$), $S(\alpha)$ was obtained by interpolation from the tabulated values (Griem 1964, Table 4-3). Elsewhere the asymptotic formulae were used (Griem 1964, eqs. [4-93], [4-94a], and [4-94b]); the values of the function $R(N,T)$ appearing in these formulae were obtained by interpolation from the tabulated values (Griem 1964, Table 4-7).

We may express the number of H ions as the difference between the number of neutral H atoms and the total number of H atoms per gram (i.e., $X/m_{\rm H}$, where $m_{\rm H}$ is the mass of the H atom and $X = 0.68$ is the abundance of hydrogen used in the model atmosphere):

$$N_{\rm H\,II} = N_{\rm H} - N_{\rm H\,I} = (X/m_{\rm H}) - N_{\rm H\,I}. \tag{10}$$

Combining this with the Boltzmann and Saha equations we can write the number of H atoms per gram in the second level as

$$N_2 = \frac{(X/m_{\rm H})\, g_2 \exp(-\chi_{2,0}/kT)}{U(T,P_e) + [2(2\pi m_e)^{2/3}(kT)^{5/2} \exp(-\chi/kT)]/h^3 P_e}. \tag{11}$$

Here, $\chi_{2,0}$ is the excitation potential of the second level, χ is the ionization potential of hydrogen, and g_2 is the statistical weight of the second level. The partition function

$U(T,P_e)$ was obtained by interpolation from the values calculated by de Jager and Neven (1957).

b) The Source Function

The Planck function is frequently used as the source function for lines such a Hβ. Scattering, however, can be important in the cores of strong lines, and it proved feasible to include this effect. When pressure broadening is the dominant mechanism, the line scattering will be almost completely non-coherent (Böhm 1960).

Unsöld (1955) has given the following approximation for the ratios of scattering to pure absorption for a transition $i \rightarrow j$:

$$\frac{\iota_\nu}{l_\nu} = \frac{A_{ji}}{\sum\limits_{\substack{k<i \\ k\neq j}} A_{jk} + \sum\limits_{l>j} B_{jl} I_\nu} . \tag{12}$$

Here, we have taken the scattering to be completely non-coherent. The A_{ij}'s and B_{ij}'s are the Einstein coefficients. This equation may also be written as

$$\frac{\iota_\nu}{l_\nu} = \frac{P_{ji}}{1-P_{ji}} , \tag{13}$$

where P_{ij} is the probability that, under conditions of local thermodynamic equilibrium, an atom in level i will make a transition to level j rather than to some other level. From

TABLE 1

APPROXIMATION PARAMETERS FOR $P_{4,2}$

k	a_k
0	−2 21920
1	+4 71304
2	−3.57918
3	+1.24568
4	−0 00038
5	−0 16315

equation (12) it is clear that for a given line P_{ij} must be a function of the radiation field and hence, in LTE, of only the temperature.

In this case we can approximate I_ν by B_ν, and it is evident from equation (12) that P_{ji} could be well approximated by

$$P_{ji} \cong \sum_{k=0}^{N} a_k \exp(5040k/T) . \tag{14}$$

Grasberger (1957) gives values for P_{ij} for Hβ at four temperatures. These values, plus the value of Unsöld at 5600° K given by Böhm (1960) and the asymptotic behavior of (ι_ν/l_ν) as $T \rightarrow \infty$, enable us to fit a six-term polynomial of the type given in equation (14). The values of a_k are given in Table 1.

Thus, we have the approximate values of (ι_ν/l_ν) for all temperatures of interest. This result, plus the values of $(l_\nu + \iota_\nu)$ from equation (7), specifies both ι_ν and l_ν at each point in the atmosphere.

The source function is taken to have the form

$$S_\nu = \frac{\kappa + l_\nu}{\kappa + l_\nu + \sigma + \iota_\nu} B_\nu + \frac{\iota_\nu}{\kappa + l_\nu + \sigma + \iota_\nu} \bar{J} + \frac{\sigma}{\kappa + l_\nu + \sigma + \iota_\nu} J_\nu , \tag{15}$$

where σ represents the contribution to the extinction coefficient due to electron scattering. The mean intensity is

$$J_\nu = \tfrac{1}{2}\int_0^\infty S_\nu(x)E_1(|\tau_\nu - x|)\,dx, \tag{16}$$

and $\bar{J}$ is the averaged mean intensity over the line defined by

$$J = \frac{\int_0^\infty \iota_\nu J_\nu d\nu}{\int_0^\infty \iota_\nu d\nu}. \tag{17}$$

Following de Jager (1952), equation (15) was solved by iteration choosing a number of frequencies, ν_k, over the central portion of the line; the line center controls the value of $\bar{J}$ due to the high value of $S(a)$ and consequently of ι_ν there.

Let

$$S_{\nu_k}^{(n+1)} = \frac{\kappa + l_{\nu_k}}{\kappa + l_{\nu_k} + \sigma + \iota_{\nu_k}} B_{\nu_k} + \frac{\iota_{\nu_k}}{\kappa + l_{\nu_k} + \sigma + \iota_{\nu_k}} \bar{J}^{(n)} + \frac{\sigma}{\kappa + l_{\nu_k} + \sigma + \iota_{\nu_k}} J_{\nu_k}^{(n)} \tag{18}$$

$$(k = 1, \ldots, 8)$$

and

$$J_{\nu_k}^{(n)} = \tfrac{1}{2}\int_0^\infty S_{\nu_k}^{(n)}(x)E_1(|\tau_{\nu_k} - x|)\,dx \quad (k = 1, \ldots, 8), \tag{19}$$

where n is the level of iteration.

The integrals of equation (17) were evaluated by an eight-point Gauss-Legendre quadrature over the frequencies ν_k; the integral in equation (19) was evaluated by a Reiz quadrature (Aller 1963). Starting with $S_{\nu_k}^{(1)} = B_{\nu_k}$, the system converges after three or four iterations (i.e., $n = 3$ or 4). In this fashion the values of $\bar{J}$ were found as a function of the continuum optical depth for each atmosphere used (i.e., for each different latitude on the star).

While the source functions at the frequencies ν_k were obtained in this process, it was not practical to determine the source function for all the necessary frequencies in this way. Thus, an approximation was made for the last term of the right-hand side of equation (15).

This approximation, due to Capriotti (1965), consists of expanding the right-hand side of equation (16) in a Taylor series and exchanging the order of integration and summation:

$$J_\nu(\tau_\nu) = \tfrac{1}{2}\sum_{n=0}^{\infty} S_\nu^{[n]}(\tau_\nu)\int_0^\infty \frac{(\tau_\nu - x)^n}{n!}E_1(|\tau_\nu - x|)\,dx \quad (0 < \tau_\nu \leq \infty). \tag{20}$$

Here, $[n]$ denotes the nth derivative.

These integrals are analytic, and evaluation of them gives

$$J_\nu(\tau_\nu) = \sum_{n=0}^{\infty} a_n(\tau_\nu)S^{[n]}(\tau_\nu), \tag{21}$$

where

$$a_n(\tau_\nu) = \frac{1}{2(n+1)}\left\{1 + (-1)^n\left[1 + \frac{\tau_\nu^{n+1}E_1(\tau_\nu)}{n!} - e^{-\tau_\nu}\sum_{k=0}^{n}\frac{\tau_\nu^k}{k!}\right]\right\}. \tag{22}$$

For our purposes, we neglect the derivatives, so we have

$$J_\nu(\tau_\nu) \cong S_\nu(\tau_\nu)[1 - \tfrac{1}{2}E_2(\tau_\nu)] . \tag{23}$$

Inserting this expression in equation (15), we obtain

$$S_\nu \cong \frac{(\kappa + l_\nu)B_\nu + \iota_\nu \bar{J}}{\kappa + l_\nu + \iota_\nu + (\sigma/2)E_2(\tau_\nu)} . \tag{24}$$

This should be a good approximation in the line center since $\sigma \ll (l_\nu + \iota_\nu)$. When the line absorption is small compared to the continuum absorption, however, we cannot expect expression (24) to be a good approximation. Hence, we have used the continuum source function from the model atmosphere wherever the continuum absorption is greater than the line absorption. This assures that the line intensity will approach the continuum intensity in the wings.

To summarize, $\bar{J}$ was computed from equations (17)–(19) for each latitude selected. Then, in the subsequent calculations approximation (24) was used where $(l_\nu + \iota_\nu) \geq (\sigma + \kappa)$ and the continuum source function where $(\sigma + \kappa) > (l_\nu + \iota_\nu)$.

c) The Integrated Line Intensities and the Residual Intensities

In the preceding sections we have expressed the source function and the line-absorption coefficients as functions of the continuum optical depth through the tabulated parameters of the model atmosphere. We now consider the intensity in the line at the surface as given by the classical solution of the equation of transfer.

$$I_\nu(0,\mu) = \int_0^\infty S_\nu(t_\nu)\exp(-t_\nu/\mu)\frac{dt_\nu}{\mu} . \tag{25}$$

We obtain the optical depth in the line, t_ν, as a function of the continuum optical depth, τ, from the definition of t_ν:

$$t_\nu(\tau) = \int_0^\tau \eta(t)\,dt , \tag{26}$$

where

$$\eta(\tau) = \frac{l_\nu + \iota_\nu + \kappa + \sigma}{\kappa + \sigma} . \tag{27}$$

The integral of equation (26) was evaluated by Gauss-Legendre quadrature:

$$t_\nu(\tau) = \tau \sum_{k=1}^{N} \eta(\tau x_k)\gamma_k , \tag{28}$$

where the x_k's and γ_k's are the appropriate roots and weights. To evaluate equation (25) the substitution

$$z = \frac{\eta(0.1)\tau}{\mu} \tag{29}$$

was made. Equation (25) then takes the form

$$I_\nu(0,\mu) = \int_0^\infty \left\{ S_\nu(\tau)\frac{\eta(\tau)}{\eta(0.1)} \exp\left[z - \frac{t_\nu(\tau)}{\mu} \right] \right\} e^{-z} dz . \tag{30}$$

The scaling factor $\eta(0.1)$ is the ratio of line absorption to continuous absorption at the point ($\tau = 0.1$) chosen to represent a mean depth of line absorption; the exponential term inside the braces should thus be a slowly varying function reflecting the change

in η with τ. This form of the equation is appropriate for evaluation by means of a Gauss-Laguerre quadrature. The correct form is

$$I_\nu(0,\mu) = \sum_{k=1}^{N} S_\nu(\tau_k)\frac{\eta(\tau_k)}{\eta(0.1)} \exp\left[z_k - \frac{t_\nu(\tau_k)}{\mu}\right]\xi_k, \tag{31}$$

where

$$\tau_k = z_k\mu/\eta(0.1)$$

and the z_k's and ξ_k's are the appropriate roots and weights.

By varying the number of quadrature points used to evaluate equations (28) and (31), it was determined that with $N = 8$ for both equations no significant change in the numerical values of the integrals occurred if the order of quadrature was increased.

The line intensity integrated over the surface of the star is given by

$$F_\nu(i,w) = R_p^2\int_{-\pi/2}^{\pi/2}\int_0^{\pi}\left[I_{\nu'}(\theta,\phi)\,x^2(\theta)\sin\theta\,\left|\frac{\mu}{\boldsymbol{g}\cdot\boldsymbol{r}}\right|\right]d\theta\,d\phi\,. \tag{32}$$

This is essentially the same as equation (12) in Paper II; the only difference is the introduction of the Doppler shift due to rotation: the $I_{\nu'}$ must be evaluated at a shifted frequency $\nu' = \nu + \Delta\nu$, where $\Delta\nu/\nu = v/c$ and v is the component of rotational velocity as seen by the observer. The correct expression for v, in terms of the quantities defined in Paper II, is

$$v = R_p\omega_c w x(\theta)\sin\theta\sin\phi\sin i\,. \tag{33}$$

The quadrature of equation (32) is carried out exactly as in Paper II. In this fashion the integrated line intensities were obtained for thirty frequencies ranging out from the line center with a spacing of 1 Å. The continuum intensities at the corresponding frequencies, F_ν cont., were obtained by interpolation from four nearby continuum intensities evaluated in the manner of Paper II.

Finally, the residual intensities are given by

$$r_\nu(i,w) = F_{\text{line}}(\nu,i,w)/F_{\text{cont.}}(\nu,i,w)\,. \tag{34}$$

d) Equivalent Widths and β-Indices

The equivalent width of a line is

$$W_\lambda = \int_0^{\infty}(1 - r_\lambda)\,d\lambda\,. \tag{35}$$

The widths of these lines were obtained by using the trapezoidal rule over the thirty frequencies for which $r_\nu(i,w)$ had been calculated.

The measurement of accurate equivalent widths, however, has not been carried out. A simpler measure of line strength is the β-index, a photoelectric method which makes use of interference filters. Since many workers have used this method lately, we expressed our profiles in terms of these indices to facilitate comparison with observations.

The β-index is defined as the difference between the magnitude of the star measured through a wide filter (half-width $\sim$ 150 Å) and through a narrow filter centered on Hβ. Many filter combinations have been used, but the half-width of the narrow filter has usually been either 15 Å or 29 Å. The intensity seen through the filter will be

$$T = \text{const.}\int_0^{\infty} t(\nu)F_\nu(i,w)\,d\nu, \tag{36}$$

where $t(\nu)$ is the transmission-curve of the filter in question. If T_w, T_{29}, and T_{15} are the intensities seen through the wide filter, the 29-Å filter, and the 15-Å filter, respectively, then the β-indices are

$$\beta_{29} = 2.5 \log (T_w/T_{29}) \quad (37)$$

and

$$\beta_{15} = 2.5 \log (T_w/T_{15}) . \quad (38)$$

The transmission-curves for the wide filter and the 29-Å filter were obtained from Crawford (1964); the transmission-curve of the 15-Å filter was represented by a Gaussian curve centered on the line. The integration was carried to 130 Å from the line center, continuum intensities being used beyond 30 Å where no line intensities had been calculated. The trapezoidal rule was used as for W_λ with an additional ten points in the continuum region.

IV. CONSTRUCTION OF FAMILIES OF MODELS

The fundamental parameters of mass, radius, and luminosity for non-rotating stars of the spectral types investigated in this study are listed in Table 2. The values were obtained from models for interiors calculated with the aid of a computer program written

TABLE 2

DEFINING PARAMETERS FOR THE NON-ROTATING MODELS

Mass ($M\odot$)	Radius ($R\odot$)	Luminosity ($L\odot$)	T_e (° K)
9 0.....	3 76	3696	23300
6.0....	2.97	900	18400
5 0....	2.68	465	16500
4 0...	2.36	198	14200

by one of the authors (Harrington). A homogeneous composition of $X = 0.68$, $Y = 0.30$, and $Z = 0.02$ was chosen for these Cowling models to match the composition of the model atmospheres. The opacity was represented by a modified Kramers' law, and the energy generation is due to the carbon cycle. The procedure which was followed was nearly identical to that given by Schwarzschild (1958). The only significant difference is that some account was taken of the radiation pressure in the core. These models should be good representations of Population I, initial main-sequence stars.

Although it is undoubtedly possible to create more realistic model interiors, such was beyond the scope of this work. It was felt that it was sufficient to have a homogeneous set of interiors on which to base this study.

In order to relate one model to another it is necessary to know how the polar radius and total luminosity of a star of given mass and chemical composition will vary as functions of rotational velocity. In the absence of a thorough study of rapidly rotating stellar interiors, Papers I and II assumed that the polar radius and total luminosity were independent of rotational velocity. These assumptions were made primarily for simplicity and illustrative purposes, and it was hoped that perhaps they would not be too far from physical reality.

Although the problem of the rotational structure was attacked by Sweet and Roy (1953), the first-order perturbation theory developed by them was inapplicable to very rapidly rotating stars. Recently the problem of stellar interiors rotating near the verge of instability has received a good deal of attention (Epps 1964; Roxburgh *et al.* 1965; Limber and Roberts 1965). Although the question of the behavior of the physical struc-

ture of rapidly rotating interiors is far from closed, the behavior of the external characteristics of such a structure is becoming clear. Thus, we shall employ some of the recent results in this field to improve the physical justification for the assumptions of the behavior of the polar radius and luminosity for a star of given mass under the influence of rotation. In addition, we shall compare the results to those obtained in Papers I and II.

Roxburgh *et al.* (1965) have demonstrated that a star of given mass will suffer a decrease in both polar radius and total luminosity for very large rotational velocities. This result is also implied by the work of Limber and Roberts (1965) and Sweet and Roy (1953). Although the model described by Roxburgh *et al.* (1965) has a different opacity than those used in this study, the effects on the total luminosity and polar radius are essentially the same as those to be expected from a more appropriate model.

Thus, we shall attempt to combine the work of Roxburgh *et al.* (1965) with that of Sweet and Roy (1953) in order to determine a correction term to the first-order formulae of Sweet and Roy (1953) which will be approximately correct at very large rotational velocities. We shall assume that the polar radius and luminosity are given by perturbation equations of the form

$$L_\omega = L_0(1 - a_1 a + a_2 a^2) , \qquad R_p(\omega) = R_p(0)(1 - b_1 a + b_2 a^2) , \tag{39}$$

where

$$a = \omega^2/[GM/R_p^3(0)] .$$

These are essentially the perturbation equations of Sweet and Roy (1953) with a second term in a^2 added. We shall determine the coefficients (a_2 and b_2) of the second-order terms by forcing agreement with the model of Roxburgh *et al.* (1965).

In order to do this it will be convenient to express the parameter a, which Sweet and Roy (1953) have found convenient to use in formulating their perturbation theory, in terms of the normalized parameter w; the fraction of the breakup velocity ω_c. With this definition of w, it is clear that we may write a in terms of w as follows:

$$a = w^2[R_p(0)/R_e(\text{breakup})]^3 . \tag{40}$$

Noting that the non-rotating equatorial radius is the same as the non-rotating polar radius, we may use the value given by the model of Roxburgh *et al.* (1965) for this ratio to establish a relationship between a and w. That is,

$$a = 0.4184\, w^2 \equiv c^3 w^2 . \tag{41}$$

If we insist that the breakup configuration is that of a Roche model, then we know that the ratio of the polar to equatorial radius at breakup is $\frac{2}{3}$, and we evaluate the second of equations (39) with the view to determining b_2:

$$R_p(\text{breakup}) = \tfrac{2}{3} R_e(\text{breakup}) = R_p(0)(1 - b_1 c^3 + b_2 c^6) . \tag{42}$$

Using the value of b_1 determined from the work of Sweet and Roy (1953) of 0.129, and the values of $R_p(\text{breakup})/R_p(0)$ given by Roxburgh *et al.* (1965), we may directly determine b_2. In a similar manner, using the value of L (breakup)$/L_0$ given by Roxburgh *et al.* (1965), and the value of a_1 given by Sweet and Roy (1953), we may directly determine a_2 in the first of equations (39). Thus, we get the two second-order equations

$$\begin{aligned} L(w) &= L(0)(1 - 0.1678\, w^2 - 0.0792\, w^4) , \\ R_p(w) &= R_p(0)(1 - 0.0540\, w^2 - 0.0547\, w^4) . \end{aligned} \tag{43}$$

If these were the only modifications that had to be made to the formulation in Paper I, the execution of the problem would be quite simple. However, the changes in polar radius implies that the critical breakup angular velocity will be considerably higher than

under the previous set of assumptions. From § II, recall that the equation for the shape of a star under rotation may be written as

$$GM/R_p(w) = GM/R + \tfrac{1}{2}w^2\omega_c^2R^2 \sin^2\theta \tag{44}$$

or

$$1 = \frac{1}{x(\theta)} + \tfrac{1}{2}w^2\left[\frac{R_p(w)}{R_e(\text{breakup})}\right]^3 x^2(\theta)\sin^2\theta\,. \tag{45}$$

Using the second of equations (43) and the Roxburgh relationship between the nonrotating radius and the equatorial radius at breakup, we can rewrite the equation (45) as

$$1 = \frac{1}{x(\theta)} + \tfrac{1}{2}w^2\left[\frac{(1 - 0.0540w^2 - 0.0547w^4)}{1.337}\right]^3 x^2(\theta)\sin^2\theta\,. \tag{46}$$

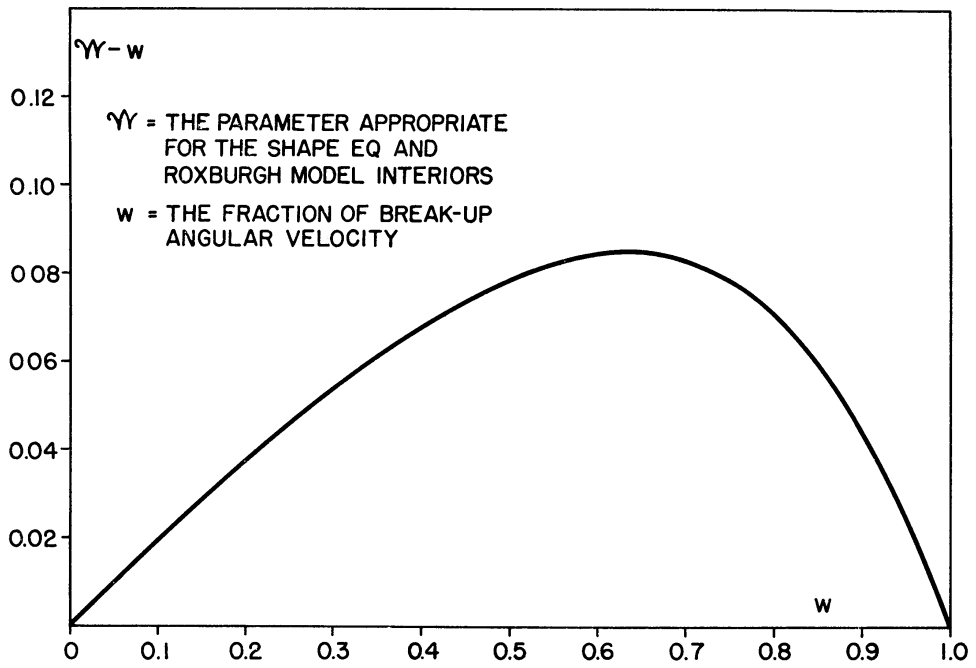

FIG. 1.—The relation of w, the fraction of break-up velocity, to ϖ, the parameter appropriate for the shape equations when R_p is a function of w.

Identifying equation (46) with equation (6), we see that, by comparing the second terms on the left-hand side of the two expressions, we may define a ϖ such that

$$\varpi^2 = \tfrac{27}{8}\, w^2[(1 - 0.0540\, w^2 - 0.0547\, w^4)/1.337]^3\,, \tag{47}$$

which will then be the appropriate normalized parameter to use in the shape equations and the expression for the normalized Von Zeipel constants C_n.

Figure 1 indicates the form of the variation of ϖ with w. It is interesting to note that ϖ is always greater than w, indicating that a star rotating at a given percentage of its breakup velocity will suffer a greater shape distortion under these assumptions than under those given in Papers I and II. This would imply that any given fraction of rapidly rotating stars would suffer a larger shape distortion than indicated in the previous work.

The specification of the behavior of the shape parameters (i.e., the radius and normalized Von Zeipel constants) with angular velocity enables us to compute the line

profile for Hβ and related parameters for the various members of a given family. It is interesting to compare the members of the families generated by equations (43) with those of Paper II, where the analogous assumptions were

$$R_p(w) = R_p(0)\,, \qquad L(w) = L(0)\,. \tag{48}$$

We might expect the extreme difference between families to occur for models rotating at or near the verge in instability. Figure 2 indicates the difference in the monochromatic magnitudes of the two families for corresponding models. It is clear that any differences in the monochromatic magnitudes in the visible region are quite small and could be considered negligible for most studies. In addition, the differences in the two sets of

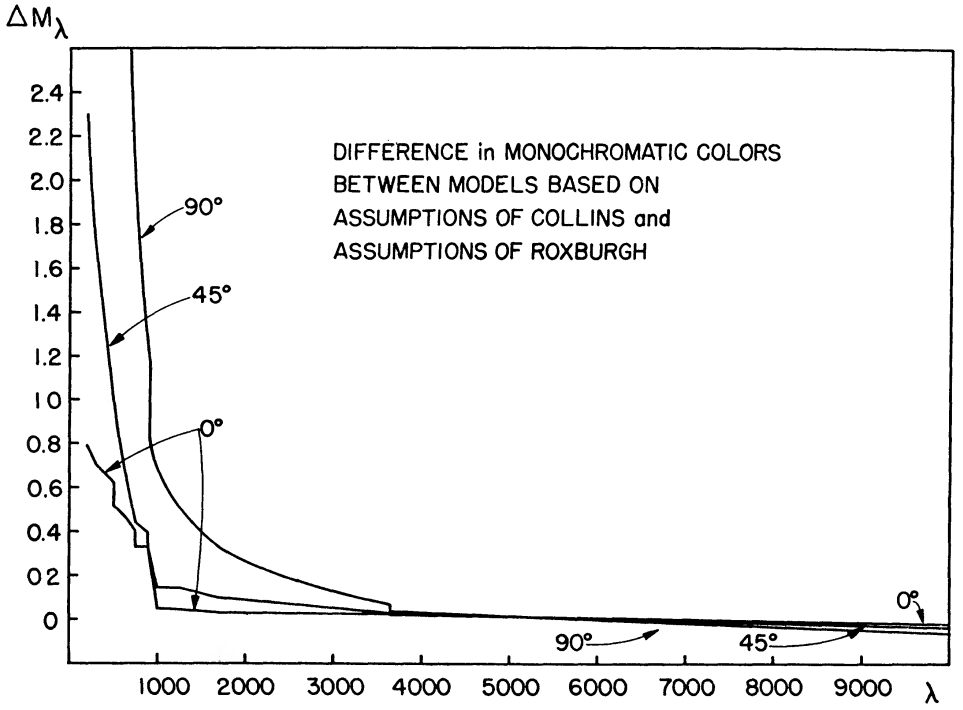

FIG. 2.—Difference in monochromatic magnitudes (normalized at λ 5040) between a family of models ($M = GM_\odot$, $w = 1.0$) with R_p = const. and a family based on calculations of Roxburgh.

assumptions produce negligible effects in the pole-on cases as far down as 1000 Å. However, for the equator-on cases the effects in the far-ultraviolet are large enough to be significant. It is tempting to try to relate the effective temperature and luminosity of these models to spectral types that one might expect such stars to exhibit. However, this is extremely difficult if the angular velocity is much different from zero. Since the MK classification scheme may be related to the physical parameters of luminosity and effective temperatures, one may do this for a small angular velocity. If the star has an appreciable rotational velocity, then effective temperatures and surface gravities appropriate for spectral classification will be given by some undetermined "average" of these parameters over the surface of the star. In addition, since the radiation field is anisotropic, the observed luminosity as determined by parallax studies will depend on the angle of inclination.

Since in this work the fundamental defining parameters for a family of models are the non-rotating values for the luminosity, mass, and polar radius, we have determined the effective temperatures of the non-rotating models and assigned spectral types from the temperatures such as given by Keenan (1963).

In the case of the rapidly rotating models, it is necessary to choose some average effective temperatures which one may hope would correspond to the effective temperature derived by means of spectral classification. It does not seem unreasonable to suppose that a suitable average would be that obtained by weighting the physical values for the effective temperature by the specific intensity at some wavelength. Thus, we shall define

$$\overline{T_e(3646+)} \equiv \int_{\text{hemisurface}} T_e(\theta,w)\, I_{3646+}(\theta,w,\mu)\, dA \Big/ \int_{\text{hemisurface}} I_{3646+}(\theta,w,\mu)\, dA\,, \qquad (49)$$

where the integral is to be taken over the hemisurface seen by the observer.

A value for the observed luminosity may be obtained from the integrated specific intensity expressed in solar units. In this work, the meaning of the term integrated specific intensity shall be the same as in Papers I and II. These two parameters were calculated for each model and are displayed in terms of a "theoretical" H-R diagram in Figure 3. It should be noted that a luminosity determined on the basis of surface gravity estimated from line strengths would be quite different from that obtained from a trigonometric parallax. Indeed, the effect of rotation on the value of this quantity as determined by the two methods will be in the opposite sense. In addition neither value will be the correct estimate of the total energy output of the star. We shall return to some of these considerations in § IV when we consider the effects of rotation on the Hβ line strength and UBV colors of the models.

V. RESULTS AND INTERPRETATIONS

No discussion of the effects of rotation on spectral line strengths would be complete without including some remarks concerning rotational effects on the continuum. Such consideration became imperative when discussing such observational parameters as Crawford's (1958) β-index or equivalent widths of the Hβ line. Even in discussing a given model we will find it desirable to relate the model to physical stars. Thus, it is necessary for us to generate, from theoretical considerations, a series of quantities which correspond to observable parameters.

In addition, if the discussion is to be fruitful, it is further required that the parameters be ones which indeed have been obtained for some large number of stars rather than just quantities which may be observed in principle. Unfortunately, the line profiles generated by this study fall into the latter category. However, they are included here in Figures 4–13 with the hope that observations of Hβ line profiles in the near future will be of sufficient accuracy to be of use in understanding rotation. Perhaps a more important reason is that these profiles contain most, if not all, the information involved in the other parameters of equivalent widths and the β-index. However, before turning to the discussion of these quantities, it would be appropriate to check the accuracy of the line profiles if possible.

Recently, in order to circumvent the absence of detailed Hβ-line information in early stars, it has become customary (Guthrie 1963; Abt and Osmer 1965) to compare theoretical predictions concerning Hβ with high quality observational material for Hγ or Hδ. Presumably, since the line absorption coefficient for Hδ has the same Stark structure as Hβ, one might expect the line profiles of the two lines to resemble each other providing they have the same equivalent width. Thus, following Abt and Osmer (1965), we shall compare a theoretical line profile for Hβ calculated for atmospheric parameters similar to those of γ Peg with observed Hδ profiles for that star (Aller 1949). The results are given in Figure 14. It should be noted that the numerical calculations are in excellent agreement with the observations even at the line center.

The comparison should be made with the dotted line rather than the computed one. Since our calculations are carried out to 30 Å from the line center, it is highly likely that Aller's choice of the position of the continuum would differ from ours. Thus, we demand-

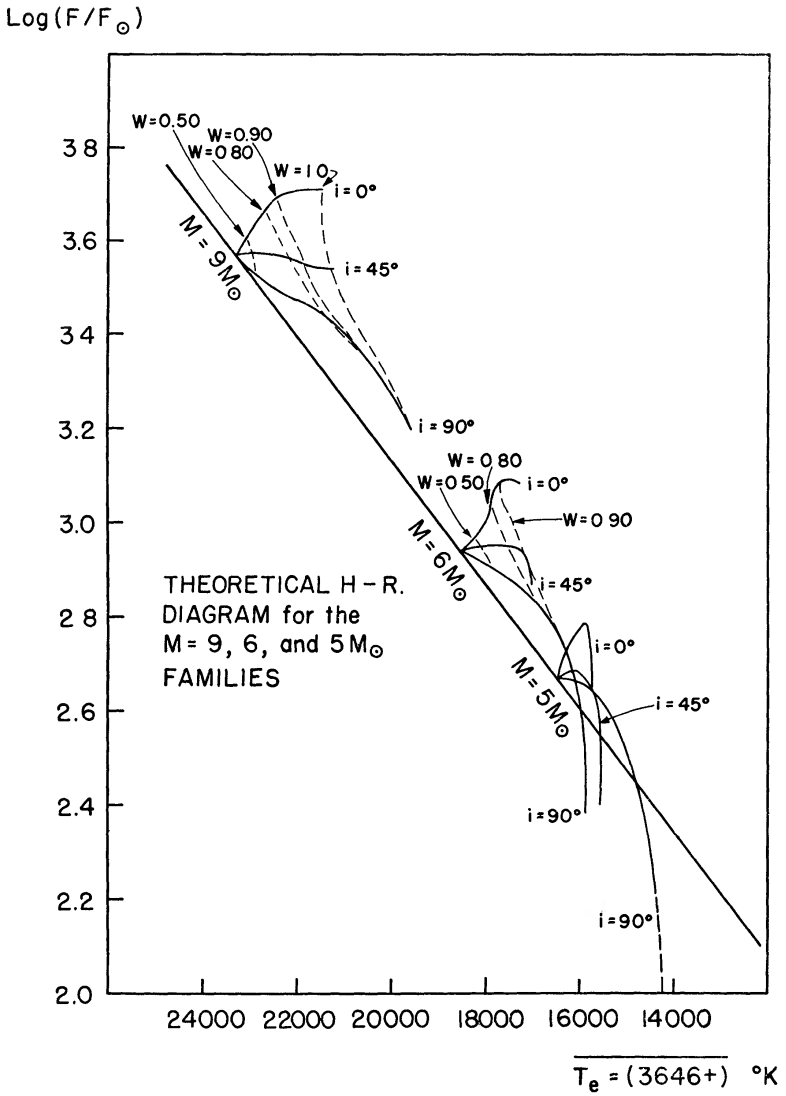

FIG. 3.—Theoretical H-R diagram for three families of models. The dotted lines connect models of equal rotational velocity. The abscissa denotes a mean value of T_e taken over the visible surface weighted by $I(3646+)$.

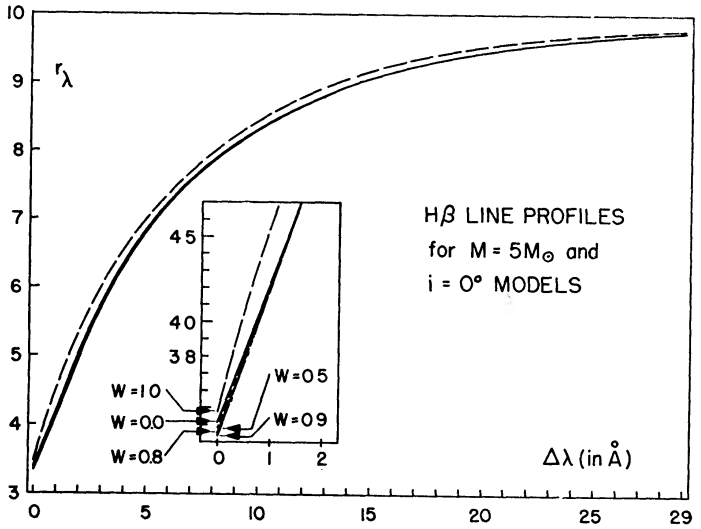

FIG. 4.—Hβ residual intensities for five rotational velocities. $M = 5\ M_\odot$ and $i = 0°$

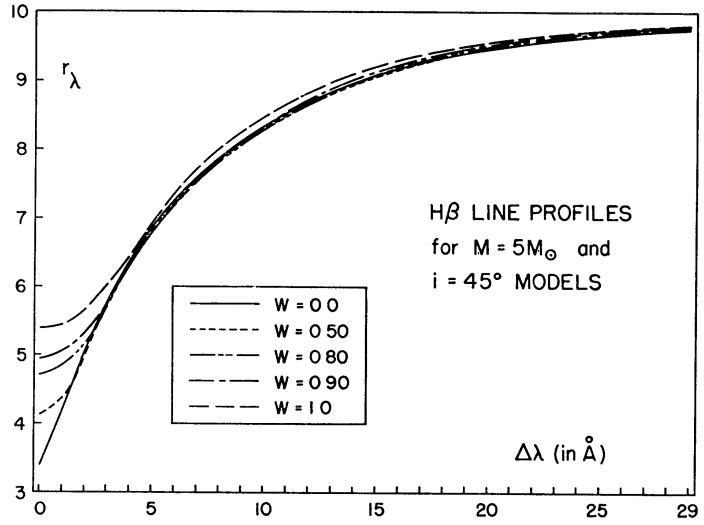

FIG. 5.—Same as Fig. 4 but with $i = 45°$

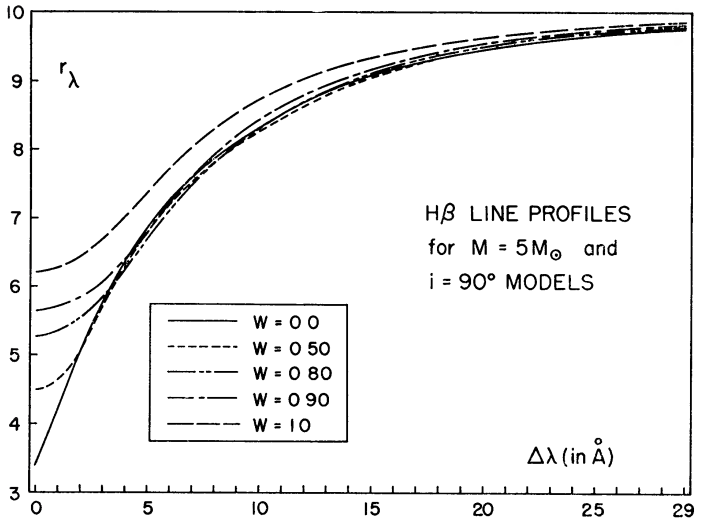

FIG. 6.—Same as Fig. 4 but with $i = 90°$

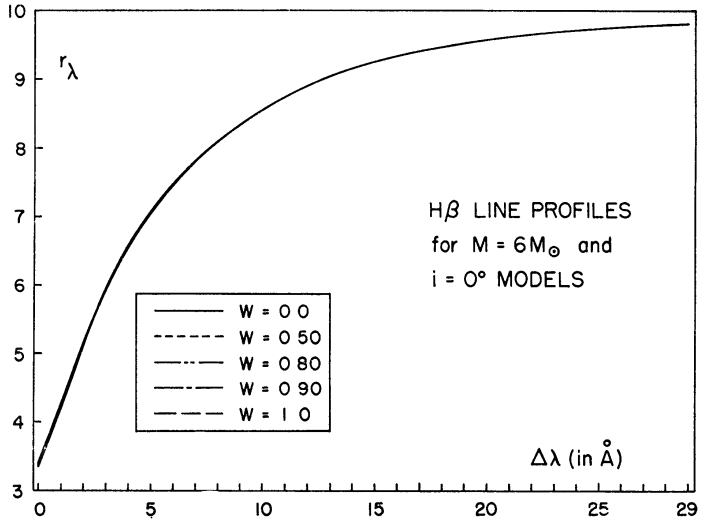

FIG. 7.—Hβ residual intensities for five rotational velocities. $M = 6\ M_\odot$ and $i = 0°$

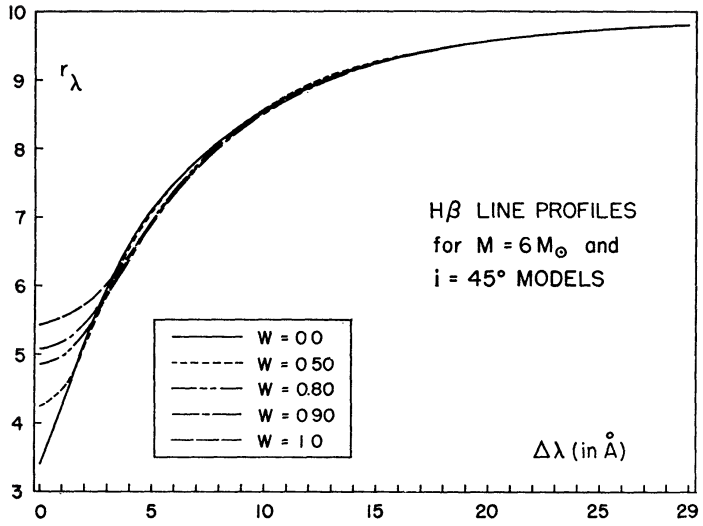

FIG. 8.—Same as Fig. 7 but with $i = 45°$

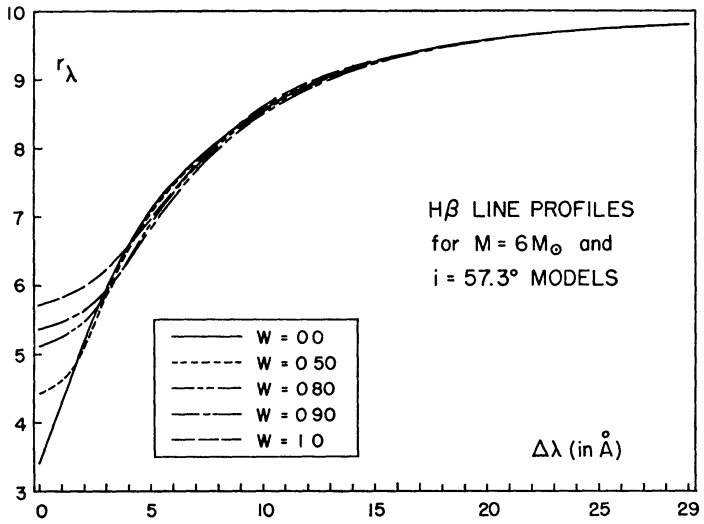

FIG. 9.—Same as Fig. 7 but with $i = 57°.3$

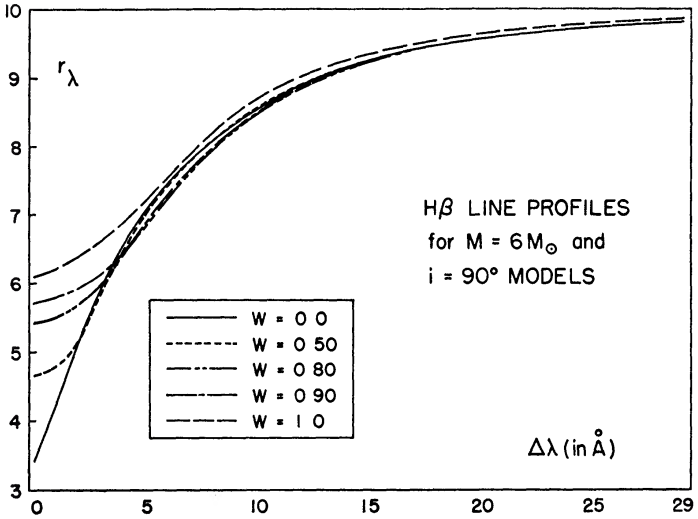

FIG. 10.—Same as Fig. 7 but with $i = 90°$

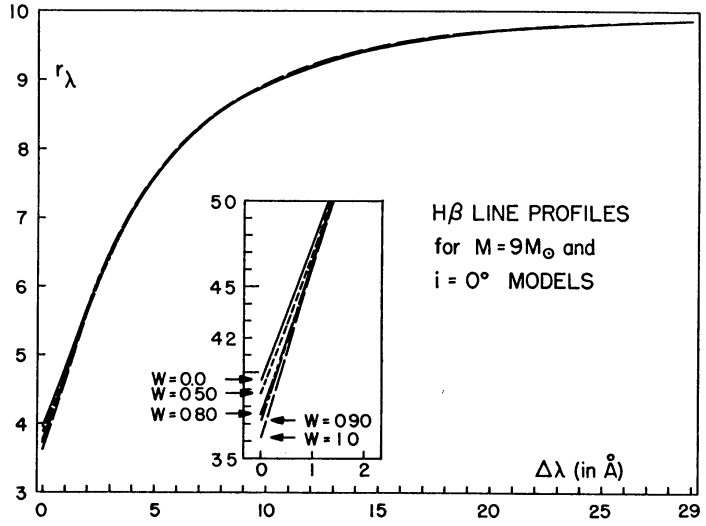

FIG. 11.—Hβ residual intensities for five rotational velocities. $M = 9\ M_\odot$ and $i = 0°$

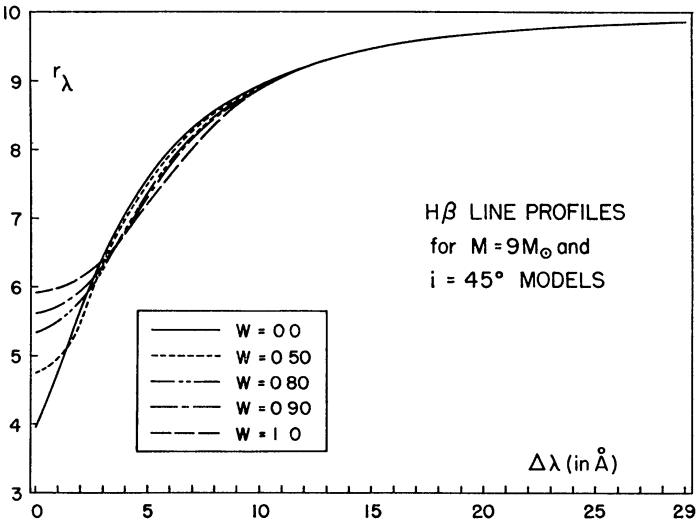

FIG. 12.—Same as Fig. 11 but with $i = 45°$

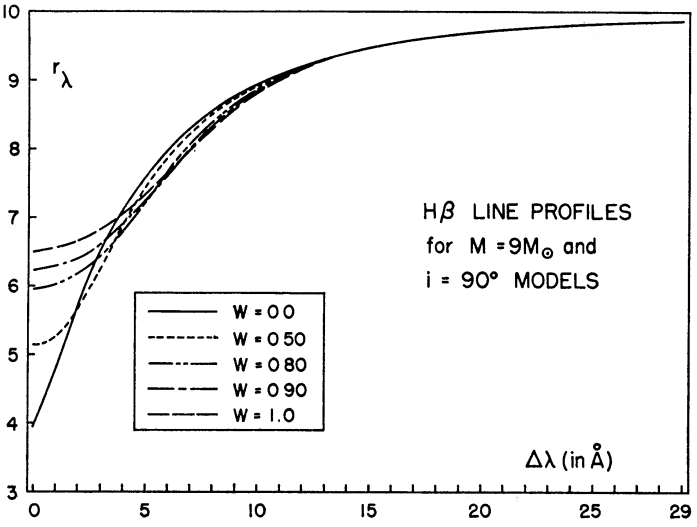

FIG. 13.—Same as Fig. 11 but with $i = 90°$

ed agreement of the profiles at 10 Å from the line center and compared the resulting shape (i.e., the *dotted line*). This also brought the equivalent width of the two lines to within satisfactory limits. Indeed the numerical value is somewhat higher than the observed one, but this could easily be due to the different ranges in $\Delta\lambda$ over which the integrations were performed. Thus, if Hδ and Hβ line profiles of comparable equivalent width are similar, we should expect the profiles and generated equivalent widths to be quite accurate. In addition to a profile for a non-rotating B2 IV star, a profile for a non-distorted but rapidly rotating B2 IV star was computed. All basic parameters such as mass, luminosity, and radius were held constant. Thus, such a line should only be geometrically broadened and the equivalent width should remain unchanged. This rotating profile is shown in Figure 14, and it was found that the equivalent widths for the two cases were indeed constant to 0.014 Å. This is a rather severe test of all the quadrature

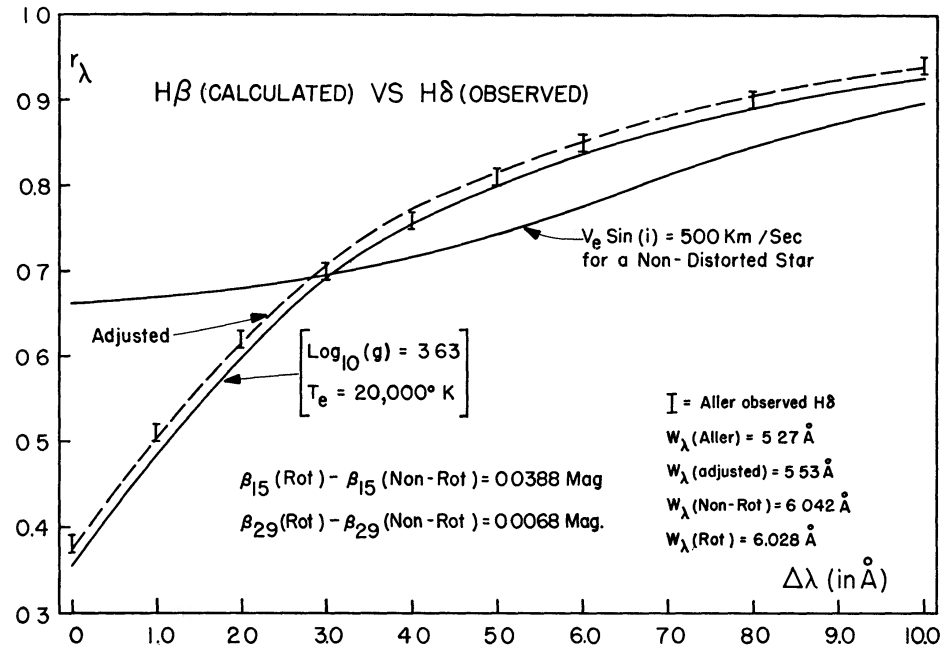

FIG. 14.—Calculated Hβ profile compared with observed values of Hδ for γ Peg. In forming the broadened profile no variations of atmospheric parameters or shape distortion were considered.

schemes used in generating the line profiles from the atmospheric parameters and the methods of calculating the equivalent widths. The rather high degree of accuracy would tend to lend credence to the quality of the line profiles themselves.

Before turning to a discussion of the large volume of material dealing with the β-index, it will be useful to investigate the effects of rotational distortion of the star on the equivalent width of the line. We shall then be in a position to decide if the variation of the β-index with v_e sin i noted by Guthrie (1963) and others is a reflection of the change in equivalent width.

In order to investigate the variation W_λ(Hβ) with rotational velocity, we must find some observational parameters akin to spectral type against which to gauge this variation. As pointed out in the previous section the notion of effective temperature is difficult to define for rotating models; thus it is not surprising that it is impossible to assign a quantitative spectral type of these models with the theory in its present state of development. Therefore, instead of spectral types we shall use the notion of photoelectric *UBV* colors. However, these quantities are difficult to put on a quantitative basis from strictly theoretical considerations in a manner which gives precise agreement with

observation (Code 1960). In spite of these difficulties, one might expect variations in the monochromatic magnitudes computed at or near the effective wavelength of the UBV filters to reflect variation of the UBV colors. Therefore, we have applied corrections to the appropriate monochromatic magnitudes computed for these models in the manner described in Paper II so that they will be in agreement with the observational colors for the stated spectral types of the non-rotating models. The colors $(U - B)_0$ and $(B - V)_0$ are then given by

$$(U - B)_0 = M\ (\lambda\ 3646) - M\ (\lambda\ 4234) - 0.83\,,$$
$$(B - V)_0 = M\ (\lambda\ 4234) + 0.79\,, \tag{50}$$

where the monochromatic magnitudes $M(\lambda)$ are referred to λ 5560. It should be noted that the corrections required to bring about agreement at spectral type B3 V also produce satisfactory agreement with the colors given by Johnson (1963) for spectral types B1 V and B5 V. Thus, we may feel confident that any changes in these predicted colors. due to rotation, lying in the B spectral class will accurately reflect observational effects.

Figure 15 indicates the position of the computed models on a color-color plot where

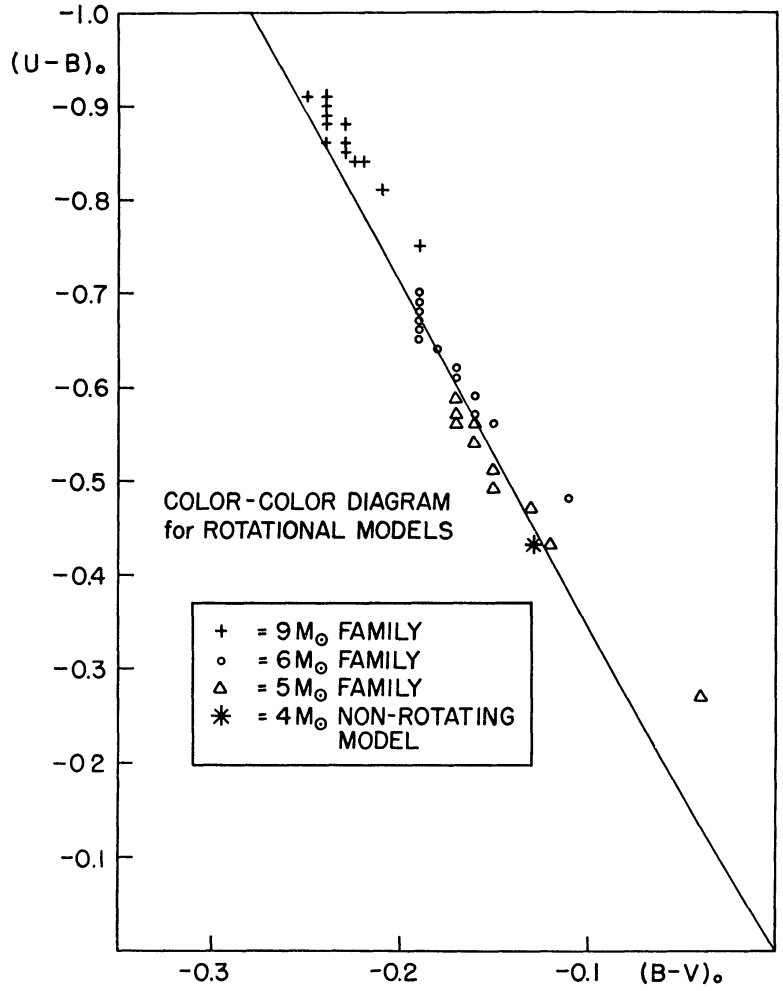

FIG. 15.—Theoretical $(U - B)_0$ versus $(B - V)_0$ plot for all models studied. The solid line is the main sequence as given by Johnson (1963).

the solid line represents the upper main sequence as given by Johnson (1963). Although the changes in the theoretical colors are often quite large, they always result in a position quite near but further down the main sequence. This is true regardless of the angle of inclination. Indeed, the rather small scatter about the main sequence is a little surprising. Thus, it appears that in the early and middle B spectral types UBV photometry will be quite ineffective in investigating the effects of rotation.

However, if we plot the equivalent widths of Hβ against $(U - B)_0$, defining a main sequence by the position of the three non-rotating models, quite another situation arises. Here the motion of a model of given mass is invariably away from the main sequence as the angular velocity increases. The amplitude of the effect is strongly determined by the angle of inclination, but the direction is not. The result of this is that we may expect a very large spread in equivalent widths for stars having the same $(U - B)_0$ due to effects of rotation. We shall define δW_λ as the difference between equivalent width the model would have if it were a main-sequence model with a $(U - B)_0$ given by the computation and the equivalent width resulting from the computation. These values were obtained from Figure 16 and are given in Table 3 and merely represent the vertical distance above the main sequence of the model.

It is clear from Figure 16 that a change of up to 50 per cent in the equivalent width of a star compared to a non-rotating star with the same $(U - B)_0$ could result from rotation. Also tracks become more non-linear with advancing spectral type. Indeed for the $M = 5\ M_\odot$ family, the initial track is nearly parallel to the non-rotational curve. Thus we would expect rotation effects on the equivalent width of Hβ to be smaller for early A stars since few of these stars have high rotational velocities. Since equivalent widths are difficult to measure and the scatter of measured values in the literature would imply the presence of large errors in their values, we shall now turn to a parameter which is closely related to the equivalent width but which can be determined with great precision. Such a parameter is the photometric β-index of Crawford (1958). In discussing the effects of rotation upon the β-index, one must consider not only the effects of rotation upon the Hβ line but also upon the continuum to which the narrow-band filter measurement is being compared. If we restrict ourselves to stars of a given $(U - B)_0$ color, we might hope that rotational effects on the continuum will be at a minimum. However, from the previous analysis of the equivalent width variations, we should then expect a large variation in the β-index with rotational velocity. This, then, is the source of the strong correlation between $\delta\beta$ and $v_e \sin i$ observed by Guthrie (1963). However, to justify this quantitatively, we must repeat the analysis similar to that used on the equivalent widths in order that they correctly include filter effects of the type discussed by Abt and Osmer (1965). In order to check the magnitude of these effects we repeated calculations of Abt and Osmer (1965) for the two profiles given in Figure 14. We found three-figure agreement for both cases. Differences between the results are probably due to the slight difference in the line strength. It should be pointed out that filter effects such as those calculated by Abt and Osmer (1965) will be a strong function of spectral type and will increase as the spectral type becomes later. For this reason we have not separately calculated this effect for each model but rather automatically included them in the calculation of the two β-indices.

Since most of the observational material available to the author is concerned with the 15-Å half-width filter, our initial analysis was in terms of this index (denoted as β_{15}). However, since this filter has been replaced with one having a 29-Å half-width in Crawford's more recent work, a parallel calculation was made for this index (denoted as β_{29}). Figure 16 indicates the computed values for the non-rotating models of both the β_{15} and β_{29} indices as a function of $(U - B)_0$. Table 3 contains the graphically determined values of $\delta\beta_{15}$ and $\delta\beta_{29}$ where $\delta\beta$ is defined in the same manner as δW_λ; that is,

$$\delta\beta = [\beta(\text{non-rot.}) - \beta(\text{comp.})]\,|_{(U-B)_0=\text{cont.}}. \qquad (51)$$

4	0	0	180.7	198.4	2.36	000.0	14169	-0.42	-0.13	0.356	10.307	10.307	+0.000	1.9232	1.9232	+0.0000	2.8896	2.8896	+0.0000

Results of H_β Line Profile and Model Calculations

$M/M_\odot$	w	i°	$F/F_\odot$	$L/L_\odot$	$R_p/R_\odot$	$V_e \sin(i)$ in km/sec	T_e(3646+)	$(U-B)_o$	$(B-V)_o$	D(w)	W_λ(w)	W_λ(o) const. $(U-B)_o$	δW_λ	β_{29}(w)	β_{29}(o) const. $(U-B)_o$	$\delta\beta_{29}$	β_{15}(w)	β_{15}(o) const. $(U-B)_o$	$\delta\beta_{15}$
9	0	0°	3854	3696.	3.76	000.0	23328	-0.91	-0.25	0.180	7.213	7.213	+0.000	1.8651	1.8651	+0.0000	2.7988	2.7988	+0.0000
9	0.5	0	4056	3523.	3.69	000.0	23100	-0.91	-0.24	0.184	7.219	7.213	-0.006	1.8657	1.8651	-0.0006	2.8009	2.7988	-0.0021
		45	3712			161.9	22898	-0.90	-0.24	0.186	7.208	7.285	+0.077	1.8649	1.8667	+0.0018	2.7965	2.8017	+0.0052
		90	3374			229.0	22802	-0.88	-0.24	0.189	7.153	7.425	+0.272	1.8630	1.8703	+0.0073	2.7898	2.8087	+0.0189
9	0.8	0	4557	3179.	3.54	000.0	22661	-0.89	-0.24	0.188	7.206	7.355	+0.149	1.8657	1.8684	+0.0027	2.8018	2.8052	+0.0034
		45	3638			277.2	22170	-0.88	-0.23	0.194	7.098	7.425	+0.327	1.8617	1.8703	+0.0086	2.7854	2.8087	+0.0233
		90	2695			392.0	21351	-0.84	-0.22	0.204	6.949	7.725	+0.776	1.8568	1.8767	+0.0199	2.7684	2.8218	+0.0534
9	0.9	0	4920	3002.	3.46	000.0	22453	-0.88	-0.24	0.190	7.173	7.425	+0.252	1.8651	1.8703	+0.0052	2.8006	2.8087	+0.0081
		45	3591			335.4	21846	-0.86	-0.23	0.198	7.036	7.570	+0.534	1.8597	1.8734	+0.0137	2.7787	2.8155	+0.0368
		90	2229			474.3	20548	-0.81	-0.21	0.214	6.789	7.947	+1.158	1.8522	1.8815	+0.0293	2.7550	2.8312	+0.0762
9	1.0	0	5403	2783.	3.35	000.0	21585	-0.85	-0.23	0.204	7.212	7.650	+0.438	1.8663	1.8751	+0.0088	2.8033	2.8187	+0.0154
		45	3518			413.8	21296	-0.84	-0.22	0.208	7.026	7.725	+0.699	1.8585	1.8767	+0.0182	2.7719	2.8218	+0.0499
		90	1580			585.3	19575	-0.75	-0.19	0.232	6.530	8.395	+1.865	1.8458	1.8908	+0.0450	2.7378	2.8486	+0.1108
6	0	0	935.4	900.6	2.97	000.0	18425	-0.70	-0.19	0.260	8.785	8.785	+0.000	1.8979	1.8979	+0.0000	2.8610	2.8610	+0.0000
6	0.5	0	989.8	858.4	2.92	000.0	18248	-0.69	-0.19	0.262	8.688	8.865	+0.177	1.8963	1.8993	+0.0030	2.8588	2.8643	+0.0055
		45	905.0			148.6	18085	-0.68	-0.19	0.265	8.654	8.940	+0.286	1.8944	1.9008	+0.0064	2.8516	2.8665	+0.0149
		57	870.3			176.8	18009	-0.67	-0.19	0.266	8.623	9.020	+0.397	1.8933	1.9022	+0.0089	2.8481	2.8686	+0.0205
		90	822.4			210.2	17895	-0.66	-0.19	0.268	8.586	9.105	+0.519	1.8919	1.9036	+0.0117	2.8433	2.8706	+0.0273
6	0.8	0	1133.	774.7	2.80	000.0	17907	-0.68	-0.19	0.265	8.708	8.940	+0.232	1.8969	1.9008	+0.0039	2.8605	2.8665	+0.0060
		45	897.9			254.4	17509	-0.65	-0.19	0.273	8.628	9.185	+0.557	1.8920	1.9049	+0.0129	2.8404	2.8723	+0.0319
		57	800.3			302.8	17275	-0.64	-0.18	0.277	8.575	9.265	+0.690	1.8900	1.9063	+0.0163	2.8330	2.8742	+0.0412
		90	663.0			359.8	16855	-0.62	-0.17	0.284	8.437	9.425	+0.988	1.8859	1.9088	+0.0229	2.8201	2.8773	+0.0572
6	0.9	0	1227.	731.4	2.74	000.0	17750	-0.67	-0.19	0.268	8.696	9.020	+0.324	1.8964	1.9022	+0.0058	2.8588	2.8686	+0.0098
		15	1180.			112.7	17719	-0.67	-0.19	0.269	8.716	9.020	+0.304	1.8960	1.9022	+0.0062	2.8557	2.8686	+0.0129
		30	1055.			217.7	17557	-0.65	-0.19	0.272	8.673	9.185	+0.512	1.8939	1.9049	+0.0110	2.8468	2.8723	+0.0255
		45	883.2			307.9	17260	-0.64	-0.18	0.278	8.585	9.265	+0.680	1.8907	1.9063	+0.0156	2.8350	2.8742	+0.0392
		57	739.7			366.4	16916	-0.62	-0.17	0.285	8.481	9.425	+0.944	1.8875	1.9088	+0.0213	2.8247	2.8773	+0.0526
		90	537.4			435.4	16225	-0.57	-0.16	0.299	8.239	9.685	+1.446	1.8811	1.9146	+0.0335	2.8072	2.8829	+0.0757
6	1.0	0	1203.	678.2	2.65	000.0	17299	-0.61	-0.17	0.288	8.517	9.500	+0.983	1.8920	1.9101	+0.0181	2.8480	2.8788	+0.0308
		45	740.0			379.8	17082	-0.59	-0.16	0.294	8.221	9.643	+1.422	1.8821	1.9126	+0.0305	2.8150	2.8813	+0.0663
		57	534.9			452.0	16766	-0.56	-0.15	0.302	7.947	9.840	+1.893	1.8750	1.9156	+0.0406	2.7965	2.8836	+0.0871
		90	243.4			537.2	15827	-0.48	-0.11	0.324	7.216	10.160	+2.944	1.8584	1.9206	+0.0622	2.7602	2.8879	+0.1277
5	0	0°	501.4	465.0	2.68	000.0	16456	-0.59	-0.17	0.296	9.643	9.643	+0.000	1.9126	1.9126	+0.0000	2.8813	2.8813	+0.0000
5	0.5	0	536.6	443.2	2.63	000.0	16300	-0.59	-0.17	0.299	9.652	9.643	-0.009	1.9124	1.9126	+0.0002	2.8807	2.8813	+0.0006
		45	495.0			142.9	16153	-0.57	-0.17	0.302	9.626	9.685	+0.059	1.9113	1.9146	+0.0033	2.8753	2.8829	+0.0076
		90	455.1			202.1	15982	-0.56	-0.17	0.306	9.559	9.840	+0.281	1.9093	1.9156	+0.0063	2.8681	2.8836	+0.0155
5	0.8	0	590.3	400.0	2.52	000.0	16006	-0.57	-0.17	0.306	9.638	9.685	+0.047	1.9120	1.9146	+0.0026	2.8793	2.8829	+0.0036
		45	458.3			244.7	15652	-0.54	-0.16	0.315	9.416	9.930	+0.514	1.9065	1.9172	+0.0107	2.8618	2.8850	+0.0232
		90	325.5			346.1	15063	-0.49	-0.15	0.328	9.091	10.125	+1.034	1.8984	1.9202	+0.0218	2.8400	2.8875	+0.0475
5	0.9	0	612.2	377.6	2.46	000.0	15888	-0.56	-0.16	0.312	9.517	9.840	+0.323	1.9094	1.9156	+0.0062	2.8742	2.8836	+0.0094
		45	418.0			296.1	15467	-0.51	-0.15	0.324	9.158	10.055	+0.897	1.9011	1.9192	+0.0181	2.8503	2.8866	+0.0363
		90	220.3			418.8	14540	-0.43	-0.12	0.350	8.547	10.290	+1.753	1.8864	1.9223	+0.0359	2.8149	2.8893	+0.0744
5	1.0	0	456.4	350.1	2.39	000.0	15756	-0.47	-0.13	0.339	8.978	10.185	+1.207	1.8986	1.9210	+0.0224	2.8532	2.8882	+0.0350
		45	248.5			365.3	15584	-0.43	-0.12	0.347	8.507	10.290	+1.783	1.8862	1.9223	+0.0361	2.8186	2.8893	+0.0707
		90	-----			517.3	14632	-0.27	-0.04	0.387	7.015	10.500	+3.485	1.8524	1.9250	+0.0726	2.7457	2.8916	+0.1459

Figure 17 describes the variation of $\delta\beta_{15}$ versus $v_e \sin i$ for all three families of models. A graph of similar effects on $\delta\beta_{29}$ would show essentially the same features. Indeed quantitative answers may be obtained for $\delta\beta_{29}$ and for $v_e \sin i < 400$ km/sec from Figure 17 by merely dividing the appropriate value of $\delta\beta_{15}$ by 2. Beyond 400 km/sec, effects such as those calculated by Abt and Osmer (1965) cause differences in the relative values of $\delta\beta_{15}$ and $\delta\beta_{29}$ which cannot be simply described in terms of their relative band passes.

We have attempted to estimate regression lines which one might obtain if one observed a larger number of stars within a given family having a random distribution of angles of inclination and Maxwellian distribution of rotational velocities. We assumed that the sample would include no stars with $w > 0.9$ or $v_e \sin i > 250$ km/sec as in this

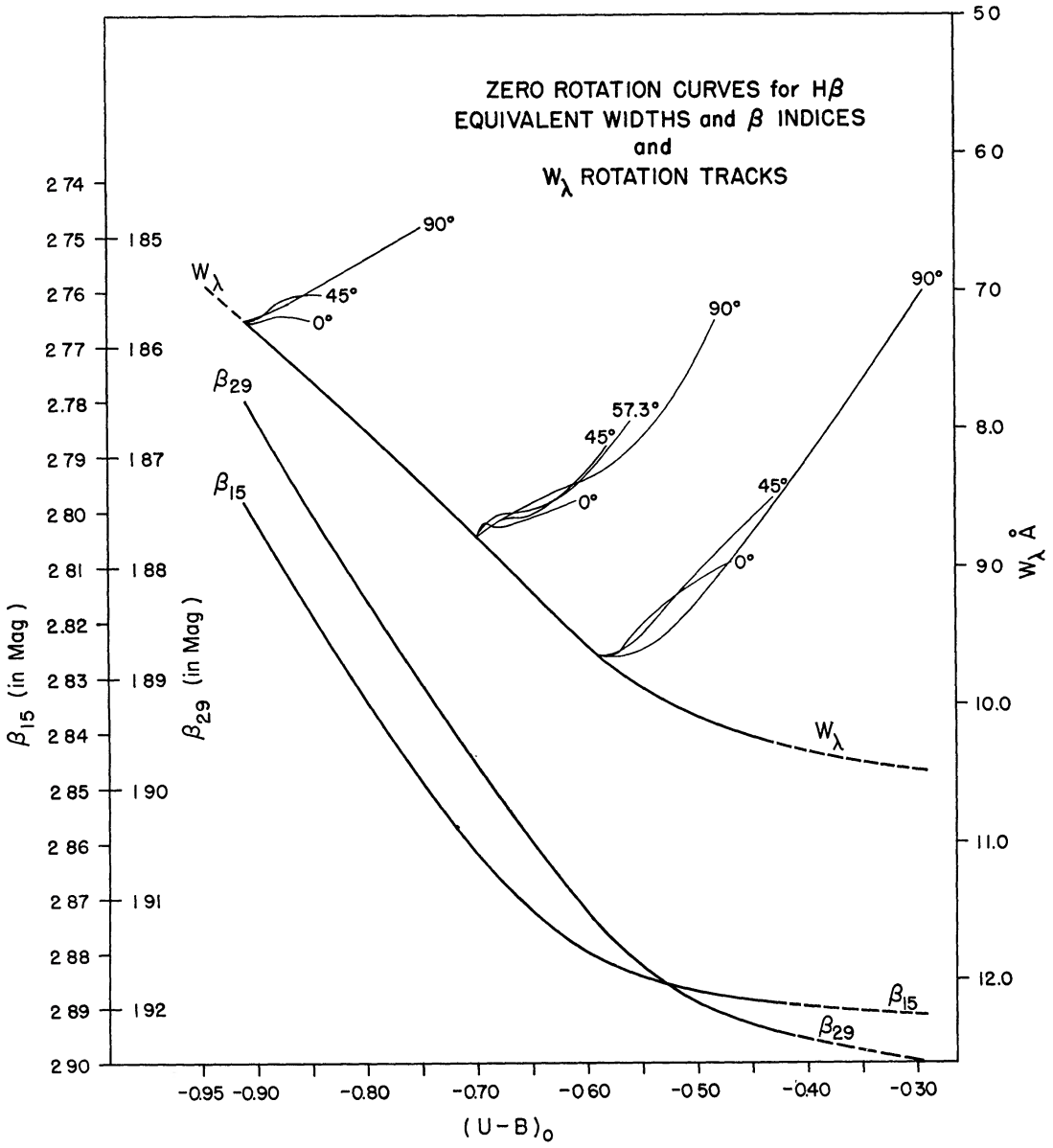

FIG. 16.—Equivalent widths of Hβ versus $(U - B)_0$ for three families. The heavy lines locate the non-rotating models; the fine lines for various angles of inclination trace the effects of increasing angular velocity up to $w = 1.0$. Also included are the β_{15} and β_{29} indices for the non-rotating models.

region the $\delta\beta_{15} - v_e \sin i$ relationships are approximately linear. The slopes of these lines and their values are displayed in Figure 17. It was hoped that the estimated slopes would agree with those observational values reported by Guthrie (1963) for the Pleiades, α Persei cluster, and the Orion association. Such was not the case. The theoretical values differed from the observed values by between 10 and 50 per cent depending on the family and cluster compared.

In searching for an explanation of this result, it was found that Guthrie had not adhered to the same sampling criteria that we used to estimate the linear regression line; that is, his sample of stars contained a significant number of stars having $v_e \sin i$ values of 300 km/sec or greater. It is clear from Figure 17 that the effect of rotation on

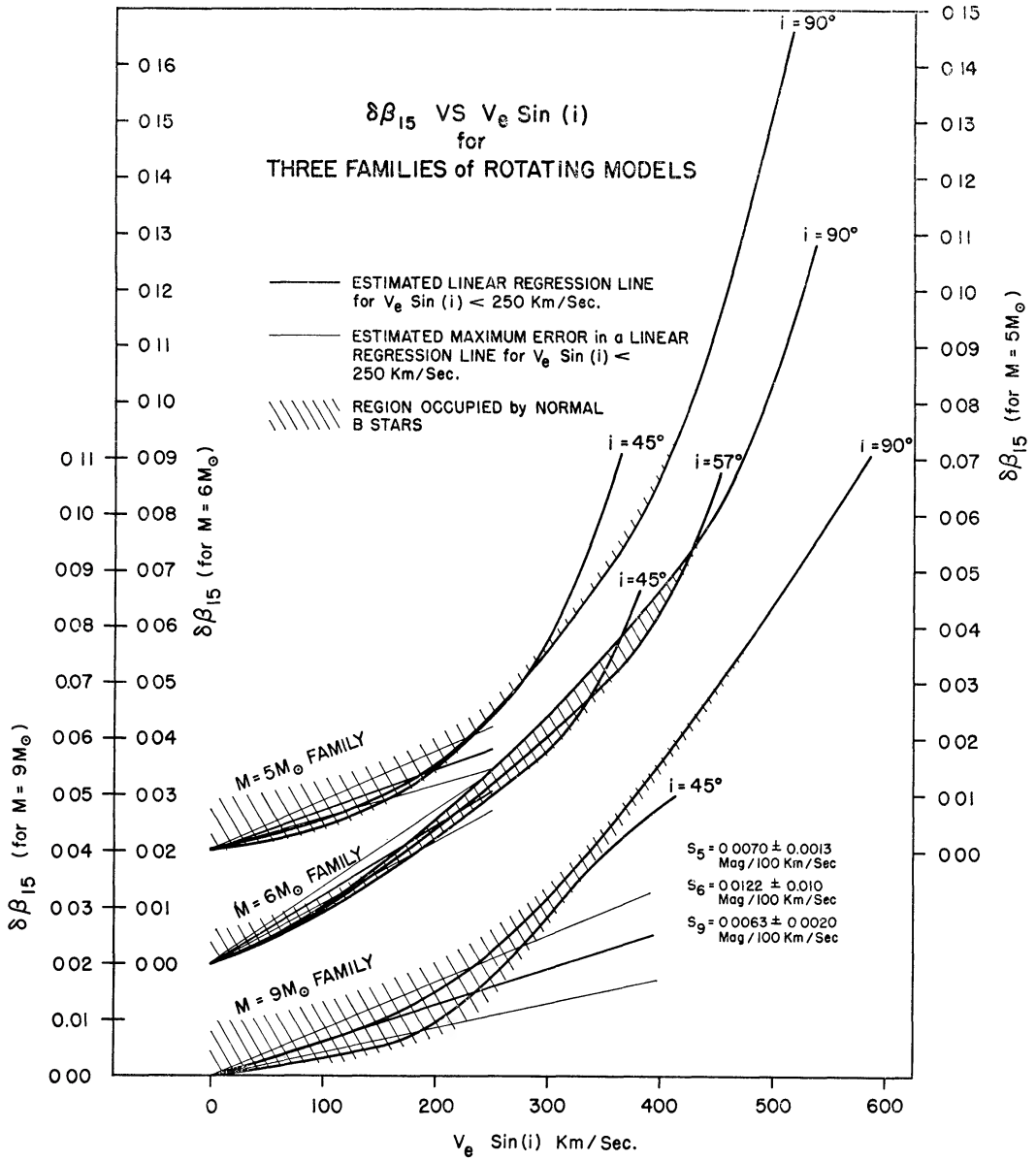

FIG. 17.—The difference, $\delta\beta_{15}$, between the β_{15} indices of the rotating models and those of non-rotating stars of the same $(U - B)_0$ color, plotted against $V_e \sin i$ for the three families.

the β_{15} index is highly non-linear. Thus the inclusion of any significant number of stars in this velocity range in an observational sample would severely bias the regression line upward.

Since it was not possible to compare the slopes of the estimated and observed regression lines meaningfully, it was decided to compare the observations themselves with the predicted region. However, even this procedure contains its uncertainties. In obtaining his values of $\delta\beta_{15}$ Guthrie (1963) merely took the value to be the residual of a particular star from a linear regression line calculated in the β_{15}-$(U - B)_0$ plane. However, we obtained an estimate of $\delta\beta_{15}$ from equation (51). If β_{15} (non-rot.) depended linearly on $(U - B)_0$, then we might expect the two estimates of $\delta\beta_{15}$ to differ by a constant. It is

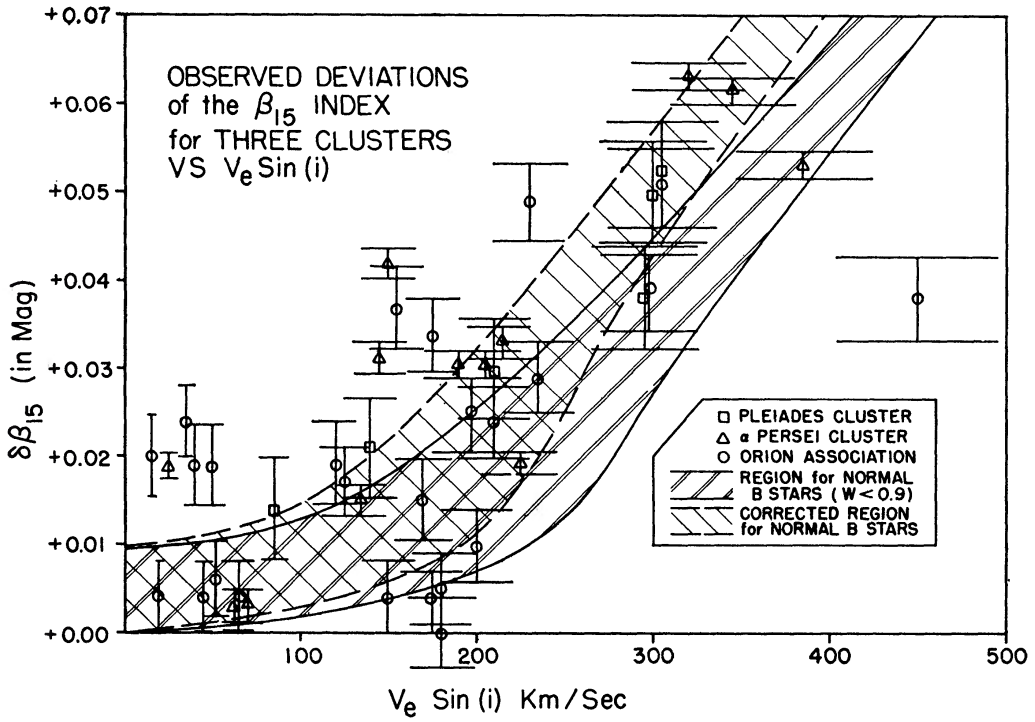

FIG. 18.—Observed deviations of the β_{15} index of cluster stars versus v_e sin i, compared with the allowed region as predicted by this study. The point at the extreme right is a suspected spectroscopic binary.

clear from Figure 16 that one could only consider the variation of β_{15} (non-rot.) with $(U - B)_0$ to be linear over fairly narrow regions of spectral type.

Fortunately, Guthrie's (1963) results for α Persei and the Pleiades satisfy this criteria. Thus, it was assumed that Guthrie's (1963) values for $\delta\beta_{15}$ and our theoretical values differed only by a constant which would be given by the ordinate intercept of Guthrie's regression lines. These transformation constants and their standard errors were obtained for the three clusters treated by Guthrie (1963). His transformed data points, with an error estimate given by the standard error in the transformation constants, are shown in Figure 18. The horizontal error estimates in v_e sin i were taken to be 10 per cent for lack of better information. Slettebak (1966*b*) indicates that this is a reasonable lower limit for the error in observationally determined v_e sin i's.

In Figure 17 we have indicated the region occupied by normal B stars for each family. For our purposes we have defined normal B stars to be those that have $w < 0.9$. This should exclude all Be stars. In Figure 18 we have indicated a similar region whose bound-

aries are defined by the extreme limits of the region in Figure 17. Thus one would expect all normal B stars to lie in this region. Inspection of Figure 18 will show that 67 per cent of the error flags of the observed stars are either cut or contained within this region. It should be pointed out that the error flags are minimum error flags and that Guthrie's sample includes some stars which probably have $w > 0.9$. A similar area for stars having $w \leq 1.0$ would contain all but one observation. This is regarded as being rather good agreement in light of the uncertainties involved. However, Figure 18 does demonstrate a tendency for the observations to lie somewhat above the predicted position. This would indicate that, although this type of theoretical approach is capable of explaining the present observations, there may well be additional effects present in these stars which we have not included in our investigation.

It is interesting to speculate on possible reasons for the systematic displacement of the observed values of $\delta\beta_{15}$ versus $v_e \sin i$ from the region expected by theory. Some of these reasons are as follows: (1) systematic differences in chemical composition between the observed sample and that used in the calculation; (2) gravity-darkening effects on the determination of observed $v_e \sin i$; (3) effects of differential rotation on the observed values of $v_e \sin i$. It seems unlikely that the first of the three possibilities would yield a discrepancy of the type observed, as it would require a large change in the abundance of hydrogen. The behavior of the other two possibilities is in the correct sense (i.e., it would make the observed $v_e \sin i$ smaller than the theoretical $v_e \sin i$. However, it is difficult to believe that the effects of gravity darkening would be important for stars rotating with $v_e < 300$ km/sec. The effect of differential rotation is not a simple one since it will affect both the calculations as well as the observed $v_e \sin i$. However, since small amounts of differential rotation will not change the shape appreciably from that which was used, we would expect the first effect to appear in the determination of the observed $v_e \sin i$.

Recently, Slettebak (1966*a*) has determined a value for the maximum rotational velocity for stars of spectral type B0–F0. He found a behavior for the breakup velocity for earlier spectral types which is similar to that predicted by this study but systematically lower. It is interesting to note that, if the abscissa of Figure 18 is contracted by the ratio of observed breakup velocities to that of the theoretical breakup velocities, the agreement between the computed and observed values $\delta\beta_{15}$ versus $v_e \sin i$ is considerably improved. Now more than 75 per cent of the error flags are cut or contained in the allowed region. Thus, it is tempting to attribute the discrepancy to systematic differences between the measured and computed values of $v_e \sin i$. This possibility will be investigated in some detail in a later paper by one of the authors (Collins).

VI. SUMMARY AND CONCLUSIONS

In this study we have attempted to present a system for accurately computing hydrogen-line profiles for rotating stars. Such line profiles are difficult to obtain because of the large and diverse number of effects affecting the result. We have attempted to consider as many effects as present theory will allow and at the same time maintain numerical accuracy.

The results have been demonstrated to agree well with observation and to provide an explanation for some of the observed effects of rotation on Hβ. We have found that rotation has little if any effect on a color-color plot of stars in the B spectral class. However, large variations in the equivalent width of Hβ may result from rotation when stars of a given color are compared. This has very serious implications for any luminosity criterion based on the strengths of the hydrogen lines when applied to stars in the B spectral class.[1] There are indications that this objection might not apply to stars of spectral type A or later.

[1] *Note added in proof.*—This point has subsequently been borne out by detailed calculation of Hγ line strengths carried out by Collins for the models described in this paper.

It appears that observations concerning the hydrogen lines offer no immediate hope in the separation of v_e from sin i due to the overlapping of a β-$(U - B)_0$ diagram of families of models having different mass. Some parameter is required which depends very sensitively on the angle of inclination but not strongly on the rotational velocity.

It has been demonstrated that this type of approach to rotational Hβ line profiles will describe most of the present observations without recourse to an *ad hoc* hypothesis. However, there is an indication that there may be effects present, such as differential rotation, which we have not considered. That these results are in qualitative agreement with those of Slettebak (1966*a*) is quite gratifying.

The authors would like to thank Dr. Roy Reeves and the staff of the Computer Center of the Ohio State University for granting the prodigious amounts of computer time required for this study. In addition their consultation and general co-operation on the project is greatly appreciated.

REFERENCES

Abt, H. A., and Osmer, P. S. 1965, *Ap. J.*, **141**, 949.
Aller, L. 1949, *Ap. J.*, **109**, 244.
———. 1963, *The Atmospheres of the Sun and the Stars* (2d ed.; New York: Ronald Press Co.), p. 220.
Böhm, K. H. 1960, *Stellar Atmospheres*, ed. J. L. Greenstein (Chicago: University of Chicago Press), p. 88.
Capriotti, E. R. 1965, *Ap. J.*, **142**, 1101.
Carroll, J. A. 1928, *M.N.*, **88**, 548–555.
———. 1933, *ibid.*, **93**, 478.
Code, A. D. 1960, *Stellar Atmospheres*, ed. J. L. Greenstein (Chicago: University of Chicago Press), p. 50.
Collins, G. W., II. 1963, *Ap. J.*, **138**, 1134 (Paper I).
———. 1965, *ibid.*, **142**, 265 (Paper II).
Crawford, D. 1958, *Ap. J.*, **128**, 185.
———. 1964, *I.A.U. Symposium 24.*
Eddington, A. S. 1926, *The Internal Constitution of the Stars* (New York: Dover Publications).
Epps, H. W. 1964, "Physical Models for Rapidly Rotating Early-Type Stars," unpublished Ph.D. thesis, University of Wisconsin.
Grasberger, W. 1957, *Ap. J.*, **125**, 750.
Griem, H. R. 1964, *Plasma Spectroscopy* (New York: McGraw-Hill Book Co.), chap. iv.
Guthrie, B. N. G. 1963, *Pub. Roy. Obs. Edinburgh*, **3**, 84.
Jager, C. de. 1952, *Rech. Astr. Obs. Utrecht*, **13**, Pt. 1, chap. viii.
Jager, C. de, and Neven, L. 1957, *Rech. Astr. Obs. Utrecht*, **13**, Pt. 4, chap. iii.
Johnson, H. L. 1963, *Basic Astronomical Data*, ed. K. Aa. Strand (Chicago: University of Chicago Press), p. 204.
Keenan, P. C. 1963, *Basic Astronomical Data*, ed. K. Aa. Strand (Chicago: University of Chicago Press), p. 78.
Limber, D. N., and Roberts, A. H. 1965, *Ap. J.*, **141**, 1439.
Roxburgh, I. W., Griffith, J. S., and Sweet, P. 1965, *Z. f. Ap.*, **61**, 203.
Schwarzschild, M. 1958, *Structure and Evolution of the Stars* (Princeton, N.J.: Princeton University Press), chap. iv, p. 15.
Shajn, G., and Struve, O. 1929, *M.N.*, **89**, 222.
Slettebak, A. 1949, *Ap. J.*, **110**, 498.
———. 1956, *ibid.*, **124**, 173.
———. 1966*a*, *ibid.*, **145**, 126.
———. 1966*b*, private communication.
Sweet, P., and Roy, A. E. 1953, *M.N.*, **113**, 701.
Underhill, A. 1951, *Pub. Dom. Ap. Obs.*, **8**, 385 (No. 13).
Unsöld, A. 1955, *Physik der Sternatmosphären* (2d ed ; Berlin: Springer-Verlag).
Von Zeipel, H. 1924, *M.N.*, **84**, 665.